

# Agricultural service unit motion planning under harvesting scheduling and terrain constraints\*

Fernando Auat Cheein<sup>1</sup>  | Miguel Torres-Torriti<sup>2</sup> | Nicolás Busch Hopfenblatt<sup>2</sup> |  
Álvaro Javier Prado<sup>1</sup> | Daniel Calabi<sup>2</sup>

<sup>1</sup>Universidad Técnica Federico Santa María, Valparaíso, Chile

<sup>2</sup>Pontificia Universidad Católica de Chile, Santiago, Chile

## Correspondence

Fernando Auat Cheein, Department of Electronic Engineering, Universidad Técnica Federico Santa María, Valparaíso, Chile.

Email: fernando.auat@usm.cl

\*This manuscript was originally submitted for the special issue on the Agricultural Robotics.

## Abstract

Most of the existing harvesting strategies rely on traditional path planners that only minimize the length of the path or energy consumption, ignoring the state of the crops and production process. Furthermore, the existing approaches use simplified kinematic models that neglect the robots' dynamics and their interaction with the terrain. To address these limitations, we propose and test in the field a harvesting and motion-planning strategy that explicitly considers the expected plant yield and the terrain's traversability. The latter has direct impact in the energy management of the agricultural service unit. A map with the predicted yield of each plant is employed to determine a priority queue of harvesting points. The priority queue, together with the harvesting rate and the robot's payload capacity, are used to generate a harvesting schedule for the different locations in the grove. The joint harvesting and motion-planning strategy applied is evaluated using field data from a Chilean avocado grove during the harvesting season. The results show that the proposed strategy provides a useful approach to automate the harvest points scheduling and motion planning while saving machinery resources.

## KEY WORDS

agriculture, planning, wheeled robots

## 1 | INTRODUCTION

At present, sustainable and economically competitive farming demands the development of more efficient agricultural production methods and technologies, thus it has become especially important to improve the harvesting and path planning of automated agricultural machinery. Autonomous robot technologies are crucial for increasing the production efficiency of agricultural processes and mitigating the mounting pressures on the environment, global food supplies, and energy resources caused by the continuous growth of the world's population. In the near future, most of the agricultural processes will require autonomous mobile robots<sup>1</sup> for a variety of tasks, such as weed detection, agrochemical application, terrain leveling, irrigation, crop monitoring, and harvesting. All of these tasks would require robots that are capable of planning their tasks and paths.

In Chile and several countries in South America, most nonintensive specialty crops that are manually harvested rely on the same strategy, i.e., field workers are assigned to crop rows (not necessarily consecutive) to collect fruits that are temporarily stored in a bin next to the plant. Once all fruits from a row have been picked, a truck collects all the bins from that row.<sup>2,3</sup> Such a harvesting strategy is

typical of fields with table grapes, avocado plantations, and olive groves, where the fruit is hand-picked from each tree. This harvesting strategy is simple to implement, but it has two main drawbacks. The first inconvenience is that some rows are harvested before other because the plants have lower yields. This generates waiting periods in which bins are not immediately taken to the storage and packing area, thus increasing the total duration of the harvest process. The second downside is that the quality of some fruits is not adequately preserved if the bins are not stored promptly.<sup>4</sup> It is therefore desirable to conceive harvesting strategies that prioritize plants according to their expected yield, taking into account the expected time required to complete the harvesting of each plant and also the payload capacity of the truck.<sup>5</sup> As pointed out in Refs. 6 and 7, very few projects involving harvesting robots use task-planning algorithms (only 6% according to the review), thus indicating the need for more research in this area.

An important aspect to improve the execution of the harvesting strategy is the adequate planning of the path between any two harvest locations in the field. In agriculture, many of the existing basic path planners do not consider the kinematic and dynamic constraints of the robot, thus generating reference trajectories that are not feasible,<sup>8,9</sup> a



problem that was overcome in the path-planning field in the late 1990s. For example, a path-planning algorithm that overcomes such a feasibility problem and is able to consider the motion model is the well-known Rapidly Exploring Random Trees (RRT) algorithm.<sup>10,11</sup> While RRT is able to find a solution very fast, this solution is not optimal, however many improvements have been made to the original RRT algorithm since its conception. One of the most interesting is RRT\*,<sup>12,13</sup> whose main advantage is the optimality of the solution and that the RRT\* is globally asymptotically optimal. An alternative variation of the original RRT algorithm was used in Ref. 14 to find obstacle-free paths for a harvesting manipulator robot.

In addition to kinodynamic constraints, terrain traversability is also an important aspect that should be considered in the path-planning stage. The terrain traversability is associated with the terramechanical parameters that affect the effectiveness of the tractive force and the wheels' slippage.<sup>15</sup> Robot terrain interaction plays an important role in rough terrain mobility. A robot traveling through dry land expends less energy than a robot traveling on clay. Considering the terrain's terramechanical characteristics, robots could adapt their control and planning strategy to minimize power consumption. One of the main problems on rough terrains is wheel slippage. The Bekker model and the Wong extension<sup>15–17</sup> are two of the most famous semiempirical terramechanics models. Several path planners incorporate a kinematic or dynamic model, but very few of these take into account the terrain/robot dynamic for planning the paths, thus generating trajectories that may not be optimal. An exception to this with nonoptimal paths can be found in Refs. 18 and 19. In the same context, when working in agricultural environments, path-planning techniques are mainly focused on covering the entire field achieving previously stated optimization criteria.<sup>4,20</sup> However, as shown there, such techniques are mostly limited to intensive crop harvesting, such as that of maize, wheat, rice, soybean, tubers, other cereals, and forage crops, which present a risk-free environment with little chance of collisions in very large areas, unlike fruit groves.<sup>21</sup> The work in Ref. 18 demonstrates the importance of considering the robot's mobility in the path-planning process due to the terrain geometry using RRT and a probabilistic approach to find safe paths on uncertain and uneven terrains. However, the approach proposed in Ref. 18 does not ensure motion efficiency because it takes into account the rollover threats instead of the wheel-ground interaction and its effects on traction and slippage. Recently, in Ref. 22, a novelty-based obstacle detection using stereo vision was incorporated into a path-planner algorithm to generate collision-free kinematically feasible paths for an agricultural robot. Nevertheless, the work focused on intensive crop harvesting, where terrain traversability is not taken into account.

The contribution of this work can be summarized in the development of an integrated harvesting and motion-planning strategy that employs information on plant yields, worker harvesting rates, and terrain traversability, and it follows the results previously published by the authors in Refs. 23 and 24. The harvesting locations in the planned route are prioritized by formulating the harvest task as a traveling salesman problem (TSP),<sup>25</sup> while the motion planning between harvesting locations is solved using the RRT\* algorithm, but including the terrain's traversability unlike the existing methods, which only consider

kinodynamic constraints and seek to ensure the path's safety. The proposed approach should be particularly useful for future autonomous robots designed to harvest specialty crops that are currently manually harvested and that possess more challenges than intensive crops.

The paper is organized as follows. Section 2 explains the standard harvesting procedure and introduces the basic notation and problem statement. Section 3 describes the proposed harvesting strategy. Section 4 addresses the path-planning approach considering traversability costs. Sections 5 and 6 provide the details of the automated service unit and the results of both the harvesting strategy and the corresponding path-planning approach, as well as a statistical analysis. Finally, the lessons learned during the experimentation and the conclusions of this work are presented in Sections 7 and 8, respectively.

## 2 | HARVESTING PROCEDURE AND PROBLEM STATEMENT

This section briefly describes the harvesting procedure typically carried out by field workers in certain specialty crops and groves that require manual labor localized at each plant. We then formulate a general problem statement and introduce the basic notation that should provide the basis for understanding the remainder of the paper.

### 2.1 | Harvesting procedure for hand-picked fruits and vegetables

Most nonintensive specialty crops—such as Hass avocado groves in Chile—that are harvested by hand labor follow the same harvesting procedure, in which the field workers collect the fruits and immediately store the product to preserve its quality.<sup>2,4</sup> Typically the collected fruits are either temporarily kept in bins close to the plant until a truck collects the bins, or directly stored in a cage hauled by a truck that moves from plant to plant until it is full. Once the truck is completely loaded, it travels to the packing area for quality control and sorting. The empty truck returns to the point where it had left and resumes the harvesting procedure. The different groups of workers start picking the fruits in any of the grove rows. Since some rows may have more fruits than others, some groups will finish sooner and will have to wait until the truck completes its route sequentially. This common harvesting strategy is simple, but it is not the most convenient for certain fruits that require immediate storage. Hence, a harvesting strategy can be conceived in such a way that prioritizes plants according to the expected yield, the expected time required to complete their harvesting, and the payload capacity, thus minimizing inadequate handling of the fruits. Figure 1 shows a general layout of the harvesting procedure implemented in this work. This procedure is described briefly as follows:

- The system uses prior knowledge of the grove. In particular, it uses previous yieldmaps, which contain information related to the productivity of the grove per square meter from the past two or three years, and the assignment of field workers and their respective alleys, made by the farmer. Yield estimation traditionally requires

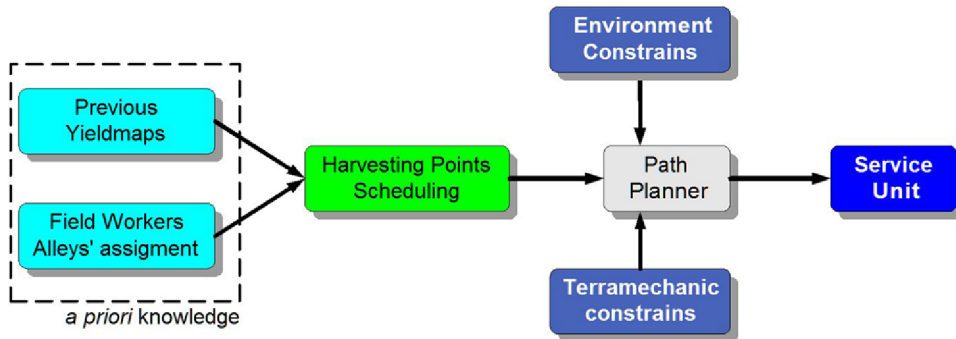


**FIGURE 1** General harvesting procedure

tedious hand measurement, which is destructive, sparse in sampling, and inaccurate.<sup>26</sup> A possible future solution to this problem in vineyards was presented in Ref. 26, where a system of cameras and illumination mounted on a vehicle automatically predicts yield accurately.

- Then, using GNSS information of the grove, i.e., the position of all harvesting points in the farm, the expected crop production per tree, and the number of field workers assigned to each row as well as the starting harvesting time, the system generates a harvesting schedule as presented in Ref. 23. Such a schedule only consists of harvesting points and the expected time when the bin will be full.
- With the previous information, the motion planner system plans the paths, taking into account the terramechanics and environmental constraints.
- Once the path and its corresponding schedule are generated, the automated service unit starts collecting the beans.

## 2.2 | Basic notation and problem statement

Let  $\mathcal{W} \subset \mathbb{R}^2$  denote a two-dimensional (2D) world with a crop or grove with  $N$  plants, e.g., trees or groups of individual smaller plants, and let  $\mathcal{L} = \{x_i | x_i \in \mathcal{W}, i = 1, 2, \dots, N\}$  denote a list of locations  $x_i$  where the plants are found. A *yieldmap* of the crop or grove is defined as a set  $\mathcal{M}_y = \{(x_i, p_i) : x_i \in \mathcal{L}, p_i = y(x_i), i = 1, 2, \dots, N\}$  of ordered pairs  $(x_i, p_i)$  of yield amounts (production) per plant  $p_i$  at each location  $x_i \in \mathcal{L}$ ,  $i = 1, 2, \dots, N$ . Similarly, a *traversability map* is defined as a set  $\mathcal{M}_\eta = \{x, \eta(x) | x \in \mathcal{W}, \eta : x \in \mathcal{W} \rightarrow \eta(x) \in \mathbb{R}^+\}$  that is associated with every position  $x \in \mathcal{W}$  a cost  $\eta(x)$  representing the difficulty of moving across that position. Let also  $x_k^r = f(x_{k-1}^r, u_k)$  be the discrete motion model for the robot, where  $f$  is the state transition function describing the motion of the robot from a state  $x_{k-1}^r$  at a time instant  $k-1$  to a new state  $x_k^r$  at a time instant  $k$  using a control action  $u_k \in \mathcal{U}$  in the set of admissible controls  $\mathcal{U}$ . The specific definition of the traversability function  $\eta$  will be introduced in Section 4. The harvesting strategy and motion-planning problem is to obtain an ordered (sorted) sequence  $S_x = (x_j \in \mathcal{L} | y(x_j) \geq y(x_i), \forall j < i, i, j \in [1, 2, \dots, N])$  that prioritizes the harvesting according to descending yield (it should be noted that this sequence begins and ends at the storage facility), and a sequence of control actions  $S_u = (u_k \in \mathcal{U} | k = 0, 1, 2, \dots, k_{\max})$ , such that the resulting trajectory of the robot  $S_r = (x_k^r \in \mathcal{W} | x_k^r = f(x_{k-1}^r, u_k), u_k \in S_u) \supseteq$

$S_x$  and some cost functional  $J : S_r \mapsto \sum_{k \in [0, k_{\max}], x_k \in S_x} d(k, x_k) \in \mathbb{R}^+$  is minimized along the path defined by  $S_r$  with some cost metric  $d : (k, x) \in \mathbb{Z}^* \times \mathcal{W} \rightarrow d(k, x) \in \mathbb{R}^+$ . In other words, the problem is to find an ordered sequence of locations  $S_x$  to be harvested, which we will also refer to as the *list of waypoints*, and a sequence of actions  $S_u$  that drive the robot along a path  $S_r$  that passes through all the waypoints in  $S_x$ . It should be noted that the set of admissible control actions  $\mathcal{U}$  depends on the load state of the robot, which is limited by its payload capacity. The dependence of  $\mathcal{U}$  on the robot's state (position and carrying capacity) has not been stated explicitly to keep the problem definition as simple as possible. However, the proposed harvest scheduling and motion-planning strategy does take into account the payload and motion constraints as explained in the next sections.

## 3 | AUTOMATED HARVESTING STRATEGY

The automated harvesting strategy employs a map  $\hat{\mathcal{M}}_y(k)$  of the predicted plant yields at current season  $k$  using information on the measured plant yields  $\mathcal{M}_y(k-1), \mathcal{M}_y(k-2), \dots, \mathcal{M}_y(k-n)$  in previous seasons  $k-1, k-2, \dots, k-n$ . For simplicity, we will refer to  $\hat{\mathcal{M}}_y(k)$  and  $\mathcal{M}_y(k)$  simply as the *predicted yieldmap* and the *measured yieldmap* at time  $k$ . The predicted yieldmap can be computed in a variety of ways. Here we employ a linearized model by Taylor's series expansion proposed in Ref. 27, in which  $\hat{\mathcal{M}}_y(k) = \alpha_2 \mathcal{M}_y(k-1) + \alpha_1 \mathcal{M}_y(k-2) + \alpha_0 \mathcal{M}_y(k-3)$ , with  $\alpha_2 = 5/2, \alpha_1 = -2, \alpha_0 = 1/2$ . However, a simple first-order IIR running average filter of the form  $\hat{\mathcal{M}}_y(k) = (1 - \alpha) \hat{\mathcal{M}}_y(k-1) + \alpha \mathcal{M}_y(k-1)$ , where  $\alpha$  is the filter update or *learning rate*, is also easy and fast to compute. The parameter  $\alpha$  can be found by iterative methods for maximum likelihood estimation, such as the expectation-maximization algorithm (see, for example, Ref. 28); in our work, we found  $\alpha = 0.128$ .

To schedule the harvesting points in  $S_x$ , it is also convenient to keep track of the progress of the harvest work. Toward that end, let  $\mathcal{M}_w = \{(x_i, w_i) | w_i \in \mathbb{R}, 0 < w_i < 1\}$  denote the *progress map* whose elements are ordered pairs of work progress  $w_i$  corresponding to the plant location  $x_i$ . Here  $w_i = 0$  means that no fruits have been collected yet, and 1 corresponds to a plant that has been fully harvested. The scheduling of points in  $S_x$  is done by formulating the problem as a TSP in which the benefit of moving from one location to the other is found as a function of the predicted yield  $\hat{\mathcal{M}}_y(k)$ , the work progress  $\mathcal{M}_w$ , the load of the

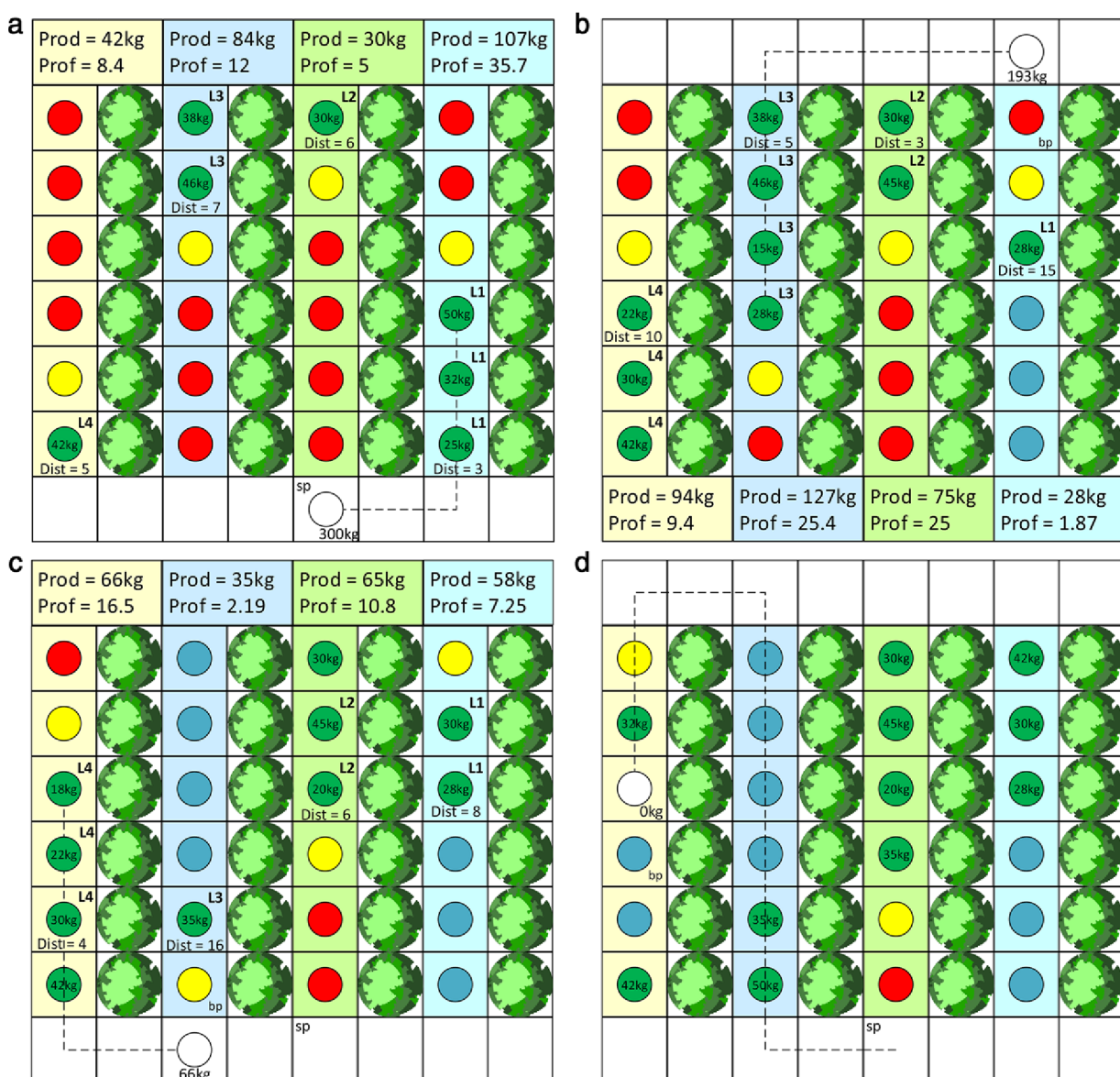


**FIGURE 2** Different snapshots of the harvesting strategy and scheduling. The robot starts harvesting according to the expected production (a), and then determining future harvesting points according to the evolution of the harvesting process status given by each bin. They are represented with three different colors: green, bins ready to be collected; yellow, bins being filled; and red, bins that are empty [see (b)-(d)]

truck Q, and the approximate distance between two points in the field, which is computed using Dijkstra's algorithm<sup>10</sup> applied to a discretized representation of the grove. The TSP is solved here using dynamic programming; see Refs. 25 and 29 for further details.

Figure 2 show different snapshots of a very small portion of a grove, like the avocado grove shown in Figure 5(b) of the next section. At the beginning, the robotic service unit is positioned outside the grove [see Fig. 2(a), white circle]. Once  $S_x$  is determined, the service unit starts collecting [Figs. 2(b)–2(d)] according to the expected harvesting evolution of each harvesting point. At this point, it is worth mentioning that the storage facility is considered to be a mandatory harvesting point with zero load by the TSP solver, thus allowing the service unit to return and begin its harvesting procedures. Figure 2 depicts the harvesting points using colors. Solid red dots are associated with trees not yet harvested, green solid dots are fully harvested plants, whereas solid

yellow dots represent harvesting in process in the specific tree (to the right of the harvesting point). Once the maximum load is reached, the service unit navigates back to the storage and packing area.

The harvesting scheduling approach can be summarized as follows:

- Avocado yield maps for three years (2012, 2013, and 2014) were provided by the agronomist. These maps contain yield information for each tree.
  - A simple linear predictor was used to estimate the amount of avocados to be harvested from each tree in 2015. More elaborate yield predictors considering other aspects, such as weather conditions, soil, and nutrients, are part of the ongoing research.
  - The amount of harvested avocados from each tree is estimated using information on the average harvesting speed of field workers. This information was provided by the agronomist.

- The TSP solver to find the ideal path between harvesting points for each navigation trial is computed taking into account each harvesting point: the predicted harvested amount, the predicted work in progress (how many avocados have been harvested according to the field workers' speed), the remaining load capacity of the service unit, and the approximated distance between two harvesting points in the field. In the approach to scheduling harvesting presented in this work, we have implemented the following as a cost function between any two adjacent harvesting points— $x_i$  and  $x_j$ —to be minimized by the TSP solver:  $x_{ij} = \epsilon_1 \hat{M}_{y,ij}^2(k) + \epsilon_2 J(S)_{x_{ij}}^2(k) + \epsilon_3 Q^2(k) + \epsilon_4 D_{ij}^2$ , where

- $\epsilon_i, i = 1, \dots, 4$  is a constant value to maintain consistency in the quadratic sum. In this case,  $\epsilon_i = 1$ , and it can be used later as a tuning parameter of the algorithm.
- $\hat{M}_{y,ij}$  is the predicted yield map of the edge  $ij$  resulting from the sum of the predicted yield for point  $i$  and point  $j$ .
- $J(S)_{x_{ij}}$  is the cost of traversing from point  $i$  to point  $j$ , according to the terrain traversability cost function given in Section 4.2.
- $D_{ij}$  is the distance between point  $i$  and point  $j$ .
- $Q$  is the current load of the bucket.

## 4 | MOTION PLANNING WITH TERRAIN TRAVERSABILITY COSTS

Terrain traversability in the context of this work is defined as the composition of efficiency losses due to the roughness of the terrain, the wheel-ground interactions, the terrain deformability, and also its slope, which together can make it more difficult for the robot to navigate along certain paths. It should be noted that by traversability here we are not referring to the accessibility or reachability of a region, the absence of obstacles along a path, or the corresponding cost to traverse it in terms of its expected length (traditional cost-to-go). Before formally stating the traversability cost, we present the robot-terrain interaction model that determines the traction efforts and losses.

### 4.1 | Robot-terrain interaction model

To account for energy losses mainly due to wheel slippage and terrain slope, we consider a simplified wheel-dynamics model given by

$$I_w \ddot{\phi}(t) = \tau_n(t) - rF_{tr}(t, \lambda), \quad (1)$$

$$m\dot{v}(t) = F_{tr}(t, \lambda) - F_{dr}(t) - F_z(t)\sin(\alpha), \quad (2)$$

$$F_{tr}(t) = \mu(\lambda)F_z(t)\cos(\alpha), \quad (3)$$

$$\lambda = 1 - \frac{v}{r\dot{\phi}}, \quad (4)$$

where  $I_w$  is the wheel's rotational inertia,  $\phi$  is the wheel's angular position,  $r$  is the wheel's radius,  $v$  and  $m$  are the longitudinal speed and mass of the mobile robot, and  $\alpha$  is the slope of the terrain. Torque  $\tau_n$  is the net traction torque applied by the motor,  $F_{tr}$  is the wheel tractive force,  $F_{dr}$  is the driving resistance, and  $F_z$  is the tire vertical load. The tire adhesion coefficient  $\mu$  depends on the road condition and the slip

ratio  $\lambda$ . For simplicity, the adhesion coefficient was approximated by a two-parameter model following Refs. 30 and 31 as

$$\mu(\lambda) = 2\mu_0 \frac{\lambda_0 \lambda}{\lambda_0^2 + \lambda^2}, \quad (5)$$

where  $\mu_0$  and  $\lambda_0$  are the peak adhesion coefficient and the slip ratio. For more accurate models, the reader is referred to Ref. 32.

Using the model equations (1)–(4), it is possible to compute the wheel slip ratio  $\lambda$  and the traction force  $F_{tr}$  for a given applied torque  $\tau_n$ . When the effective translational velocity decreases in relation to the tangential velocity of the spinning wheels, i.e.,  $v \ll r\dot{\phi}$ , the slip ratio increases, i.e.,  $\lambda \rightarrow 1$ . Thus it is possible to consider the slip condition as a loss in the efficiency to produce useful mechanical work. More precisely,  $1 - \lambda$  can be seen as the velocity efficiency of the robot. Another aspect affecting the mobility of the machine is the slope of the terrain. A positive slope  $\alpha > 0$  can be regarded as a factor reducing the efficiency, while a negative slope  $\alpha \leq 0$  can be assumed to produce no effect on the overall efficiency of the robot. Therefore, it is possible to conceive a mobility efficiency given by

$$\eta = \begin{cases} \cos(\alpha)(1 - \lambda), & \alpha > 0, \\ 1 - \lambda, & \alpha \leq 0. \end{cases} \quad (6)$$

Assuming that the robot is required to drive at its maximum speed, the mobility efficiency decreases the achievable speed to a value

$$v = \eta v_{max}, \quad (7)$$

which in turn increases the time it takes to traverse a certain region. This fact can be used to define a traversability cost function that takes into account not only the distance and the presence of obstacles along a path, but also the difficulty in driving across the region due to mobility efficiency losses.

### 4.2 | Terrain traversability cost

The traversability cost function can be defined in terms of the length of the trajectory and the time it takes to drive along a given path. Assuming that the robot delivers a constant amount of energy between any two consecutive points from the path, the minimum-time path is equivalent to the loss-minimizing path. The combination of these two costs represents the total motion effort arising from the path as well as the variations in the traction efficiency due to changes in the terramechanical properties while moving across a region in the field. Denoting by  $q = [x, y, \theta] \in Q$  the robot's state in configuration space  $Q$ , and defining a path  $S_q = \{q : \dot{q} = f(q, u), u \in U\}$  as the evolution of  $q(t)$ ,  $t \in [t_0, t_f]$  for a given motion model  $f : Q \times U \rightarrow Q$  and control  $u \in U$  the set of admissible controls, the traversability cost function can be stated as

$$\begin{aligned} J(S_q) &= k_1 \int_{s \in S_q} ds + k_2 \int_{s \in S_q} dt \\ &= k_1 \int_{s \in S_q} ds + k_2 \int_{s \in S_q} \frac{1}{v(s)} ds \\ &= k_1 \int_{s \in S_q} ds + k_2 \int_{s \in S_q} \frac{1}{\eta(s)v_{max}} ds \end{aligned}$$



**FIGURE 3** Detailed description of the sensors' placement in the miniloader

$$\begin{aligned} & \approx k_1 \sum_{k=0, x_k^r=q(kT)}^N d(x_k^r, x_{k-1}^r) + k_2 \sum_{k=0, x_k^r=q(kT)}^N \frac{1}{\eta(x_k^r) v_{\max}} d(x_k^r, x_{k-1}^r) \\ & \approx \sum_{k=0, x_k^r=q(kT)}^N \left( k_1 + \frac{k_2}{\eta(x_k^r) v_{\max}} \right) d(x_k^r, x_{k-1}^r), \end{aligned}$$

where  $d(x_k^r, x_{k-1}^r)$  is the distance between  $x_{k-1}^r$  and  $x_k^r$  (current and past position of the robot), and  $k_1, k_2$  are the penalty weights for the path length and the mobility efficiency due to terrain conditions. The last two lines of the cost functions correspond to the discrete approximation of the path replacing the integrals by summations of the trajectory sampled every  $T$ , or equivalently a trajectory partitioned in  $N = k_{\max} - 1$  subintervals.

#### 4.3 | Motion model for path planning

The motion model is considered as part of the path-planning problem in order to ensure that the controls produce trajectories that satisfy the motion model. For simplicity, and to reduce the computational burden, the motion model employed here considers the kinematic equations of a popular differential-drive robot, which in discretized form  $x_k^r = f(x_{k-1}^r, u_k)$  is given by

$$\begin{bmatrix} x_{k+1} \\ y_{k+1} \\ \theta_{k+1} \end{bmatrix} = \begin{bmatrix} x_k \\ y_k \\ \theta_k \end{bmatrix} + \begin{bmatrix} \lambda_v v_k \cos(\theta_k) T_s \\ \lambda_v v_k \sin(\theta_k) T_s \\ \lambda_w w_k T_s \end{bmatrix}, \quad (8)$$

where  $x_k^r = [x_k \ y_k \ \theta_k]$  is the state of the mobile robot at time instant  $k$  consisting of the global position and orientation,  $v_k$  and  $w_k$  are the longitudinal and angular velocities,  $\lambda_v$  and  $\lambda_w$  are longitudinal and angular slippage factors, and  $T_s$  is the sampling time. For the kinematic model of the differential drive robot, the inputs are the left- and right-wheel velocities, which are related to the longitudinal and rotational velocity by  $v_k = \frac{v_{\phi_r} + v_{\phi_l}}{2}$  and  $w_k = \frac{v_{\phi_r} - v_{\phi_l}}{L}$ , where  $L$  is the width of the robot. This model is also a good approximation to the kinematic model of skid-

steer mobile bases. If the control input is directly the longitudinal and angular velocities  $v_k$  and  $w_k$ , then the equations correspond to that of the kinematic model for a unicycle.

#### 4.4 | Path planning with terrain traversability costs

In this work, we have implemented a RRT\* path-planning approach proposed in Ref. 12 and modified it to include the traversability cost function. The aim of the RRT\* algorithm is to obtain a path  $S_x$  (the list of scheduled harvesting points); see Section 3. The RRT\* planner finds a feasible path among the harvesting points in  $S_x$  using as a cost function the traversability cost between such harvesting points, as presented in Section 4.2, instead of the traditional Cartesian distance. Further details regarding the implementation of the RRT\* path-planning algorithm can be found in Ref. 12.

### 5 | EXPERIMENTAL MATERIALS AND DESIGN

This section shows the experimental setup (the automated service) unit used in this work. Figure 3 shows the robotized service unit used in this work: a Caterpillar Cat 262C compact skid-steer loader. This machine has a 73 HP diesel engine that drives a hydrostatic inline axial piston pump. The pump runs continuously with the engine throttle held at a fixed position (i.e., it is not actuated), thus delivering a constant hydraulic power. The hydraulic force is directed to two hydrostatic axial piston motors, one on each side of the machine, by manipulating the signal of the three-way servovalves that allow control of the flow of the hydraulic fluid. The manipulated variable is set to a fixed value, which results in a constant longitudinal velocity after the short transient. Since in this open-loop mode there is no control on the velocity, the velocity of the machine slows down when the terrain is muddy or has loose soil. Therefore, the effective velocity can be assumed to be

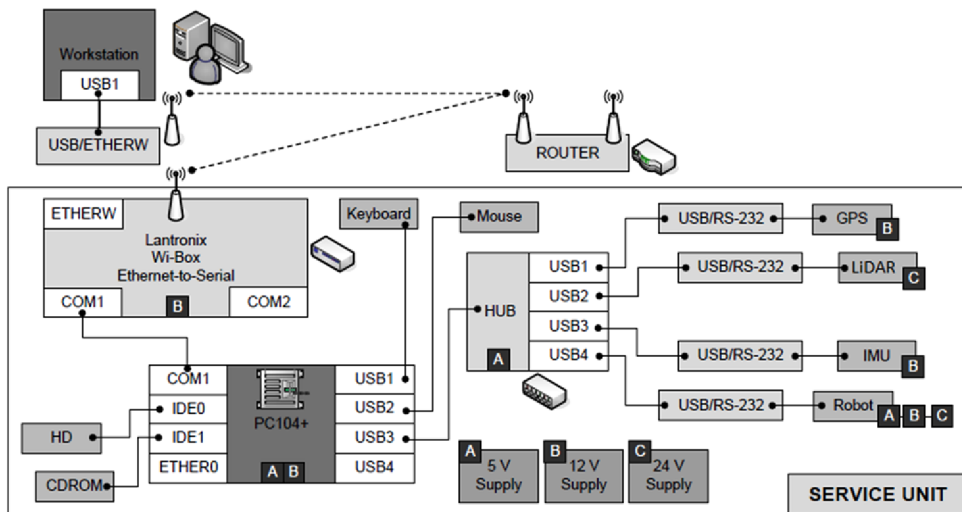


**FIGURE 4** Architecture of the automated service unit

proportional to the maximum open-loop velocity (fixed-value because of the machine operating characteristics) and the terrain's mobility efficiency in Eq. (6), which depends on the terrain's slope angle and slippage/terramechanical characteristics. Although originally designed for construction and mining tasks, the compact skid-steer vehicle shown in Figure 3 was used for the experimentation presented in this work, using the bucket as a fruit deposit.

The vehicle hardware architecture is shown in Figure 4. Its maximum longitudinal speed is set by software to 3 m/s, whereas its angular speed is set to 30 deg/s. The vehicle employs the robot operating system (ROS) on the onboard navigation computer, which is implemented using an Advantech UNO-3082 industrial PC. The mobile platform can be configured for both teleoperation and autonomous navigation. The sensor suite includes four Sick LMS-511 LiDARs, one on each side of the machine, two Vectornav VN-200 IMU/INS (GPS-aided) units, a Swiftnav Piki Global Navigation Satellite System (GNSS) receiver with centimeter-level relative positioning RTK-GPS functionality, and encoders on each hydraulic-motor driven axle. An extended Kalman filter (EKF) running in the navigation computer enables the fusion of the inertial measurement unit (IMU), GNSS, and dead-reckoning signals for position estimation, as shown in Ref. 33. Nevertheless, other approaches can be implemented using the LiDARs, such as simultaneous localization and mapping (SLAM) algorithms, which were not employed in the experimental validation of the proposed approach.

The experiment was carried out in an avocado grove of  $\sim 9$  hectares, but only 2 hectares were used. Each hectare consisted of 10 alleys of 9 m width. The grove was approximately 15 years old. Further agro-nomic details of the grove can be found in Ref. 23.

## 6 | RESULTS

### 6.1 | Motion planning with and without considering the terrain

Matlab® was used to implement the RRT\* algorithm, based on the code presented in Ref. 34. To represent the effects of the terrain on the

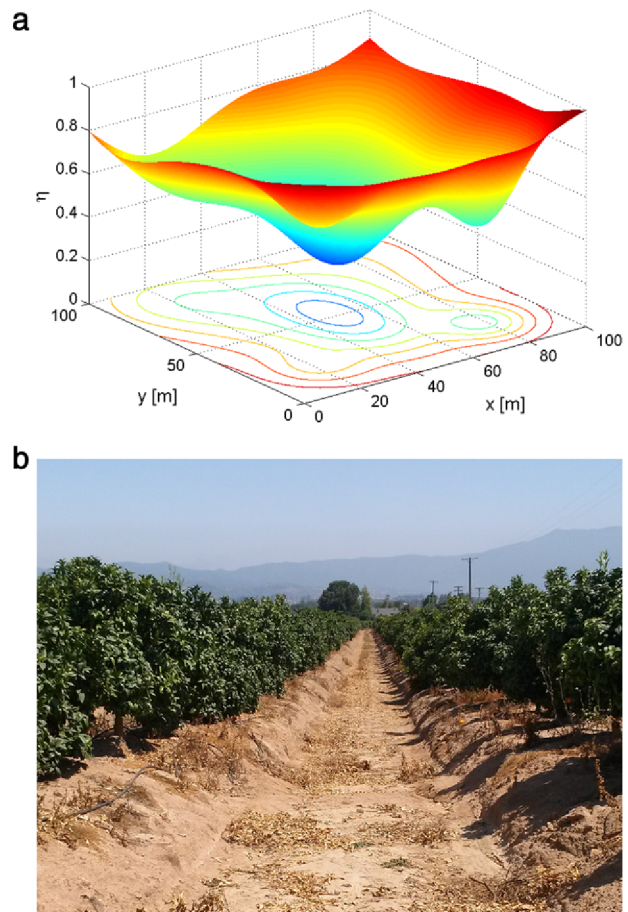


**FIGURE 5** 3D representation of  $\eta$  over the space (a) provided by the INIA-Chile, and real-world agricultural field used to generate the map (b)

robot, we generated a map of the mobility efficiency  $\eta$  [see Fig. 5(a)]. The value of the mobility efficiency  $\eta(x)$  at each point  $x \in \mathcal{W}$  ranges between 0 and 1. Regions with low mobility efficiencies  $\eta$  cause significant reductions in the robot's velocity, and hence its total travel time is increased. It is worth mentioning that the terrain characterization

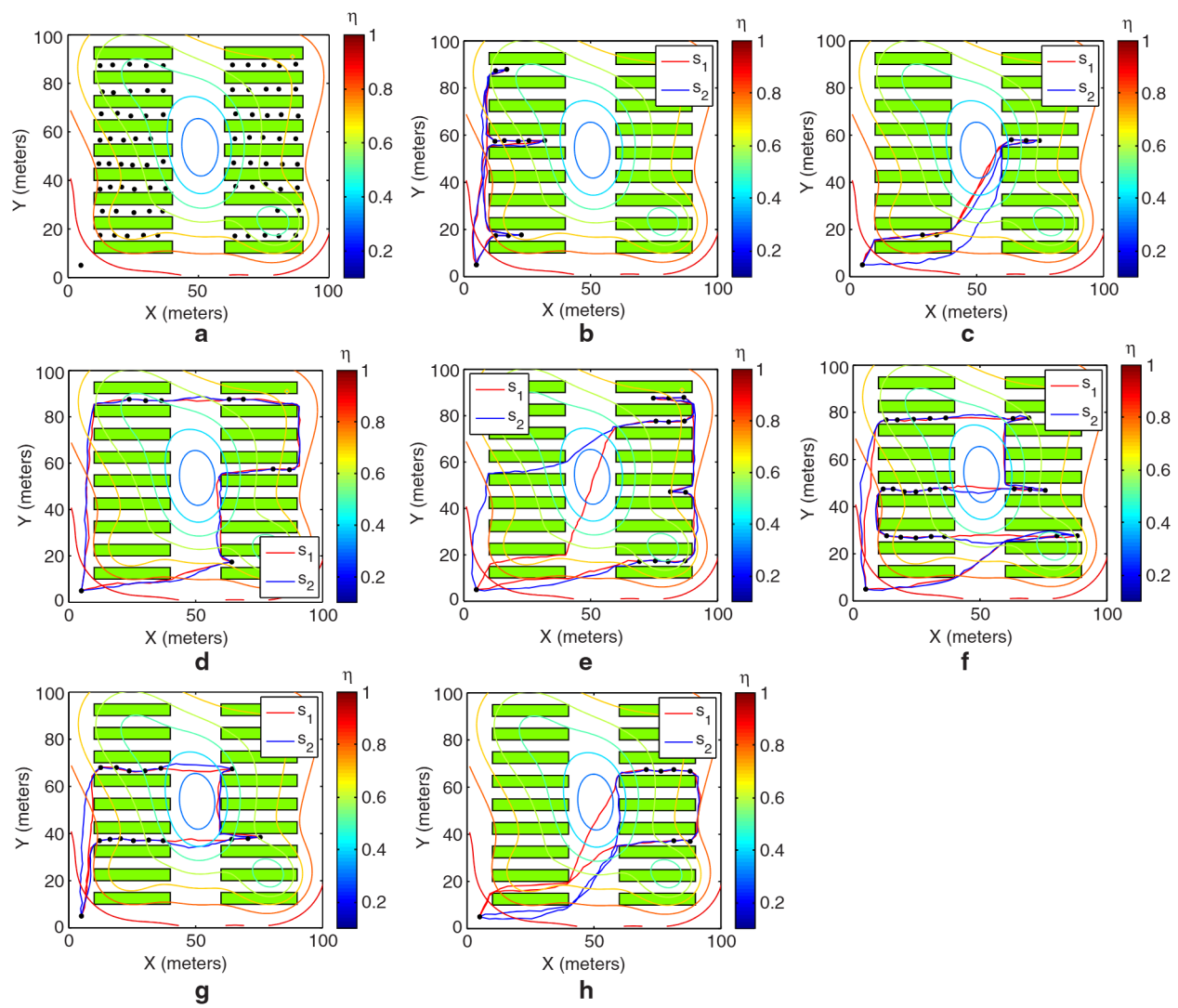


**FIGURE 6** RRT\*-based path planning in different stages of the harvesting process

shown in Figure 5(a) was provided by the INIA (the National Institution for Agricultural Research from Chile, [www.inia.cl](http://www.inia.cl)).

Using data from an avocado grove in the north of Chile, shown in Figure 5(b), a simplified map with obstacles was generated. This map considers consecutive rows of trees, separated by corridors where the robot is able to drive. The complete description of the grove considers the obstacles, the plant locations, and the terrain properties given by the mobility efficiency map.

Figure 6(a) shows all the harvesting points, which are separated in groups and sorted using the harvesting strategy proposed in Section 3. In this trial, the storage and packing area from where the robot starts is located near the coordinate origin in the bottom left part of the map, as shown in Figure 6. In the experimentation, we consider an avocado grove and a 300 kg payload capacity automated service unit. Once the system predicts that 300 kg of avocados are ready to be collected, the RRT\* approach is used to plan the path following the waypoints sorted in  $S_x$  by the proposed harvesting strategy. Figures 6(b)–6(h) show seven consecutive snapshots that cover all the harvesting positions shown in Figure 6(a). Each figure represents a route in which about 300 kg of avocados are harvested.

## 6.2 | Evaluation of the service unit in a harvesting operation

To evaluate the robot's performance, two paths are planned for the waypoints in each of the Figures 6(b)–6(h). One path is planned using the standard minimal distance metric, while the other employs the traversability cost function. The resulting paths are labeled  $s_1$  and  $s_2$ , respectively. Table 1 shows the cost  $J$  evaluated along both of the trajectories,  $s_1$  and  $s_2$ . The cost of the minimal length trajectory  $s_1$  is higher than the cost of trajectory  $s_2$ , which considers the terrain effects. It is clear from Table 1 that for every trip of the robot to a harvesting location, the cost of the optimal trajectory that considers the terrain characteristics is lower than that of the minimal length path. An illustrative case can be seen in Figure 6(e), which shows that the two paths found differ notably. This is due to the low efficiency zone at the center of the grove, indicated by the blue contour lines. When the terrain characteristics of the zone with a higher traversability cost is considered, the trajectory  $s_2$  seeks a more efficient area of the terrain. In contrast, the trajectory  $s_1$  crosses through the bad area because it ignores the terrain's traversability, thus resulting in a path of higher mobility costs.

**TABLE 1** Total cost of the trajectory obtained with different traversability costs along the minimal length path  $s_1$  and the mobility optimized path  $s_2$

Schedule	$J(s_1)$	$J(s_2)$
b	582.7	582.2
c	592.0	571.6
d	823.2	819.8
e	901.7	861.3
f	1205.0	1197.4
g	743.8	734.5
h	695.8	671.2
Total	5544.2	5438.1
$\mu$	792.0	776.9
$\sigma$	215.6	215.6

The average reduction in cost with respect to the minimal length path that does not consider the terrain characteristic is 2.0%.

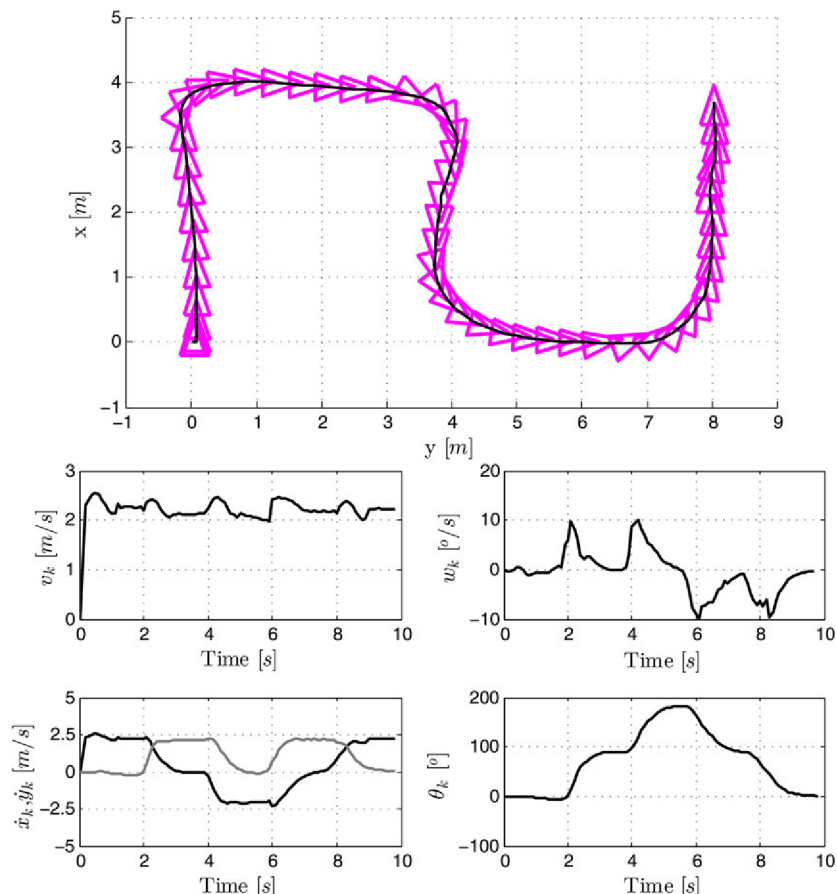
### 6.3 | Evaluation of the path-tracking performance

Figure 7 shows a single navigation case, where the path was produced by the motion planner according to the terrain parameters of the pre-

vious case, shown in Figure 5. The vehicle followed the s-shaped path using the path-tracking controller previously published by the authors in Ref. 24. For such an experiment, the total effort of the controller—as introduced in Ref. 24—is 13% smaller when compared to the case without considering the terrain conditions. However, in both cases, the total tracking error remains within the same boundaries.

### 6.4 | Harvesting efficiency evaluation

One of the main hypotheses of this work is that our system can enhance resource management by including the terramechanics constraints of the terrain in the harvesting process. Therefore, we have run several trials in order to quantify the amount of actual resources saved using our proposal. To do so, we have implemented the motion planner RRT\* used in this work with and without considering the terrain constraints. Up to 10 trials were run in the environment shown in Figure 6, each one with different harvesting points. In turn, each trial was repeated 10 times. It is worth mentioning that this experimentation was not related to harvesting, but to see if our system actually saves energy. Instead of measuring the amount of gas used by the vehicle, we calculate the control effort as presented in a previous work of the authors,<sup>24</sup> which is a direct representation of the kinematic energy of the vehicle. In particular, the accumulative control effort can be defined as the velocity



**FIGURE 7** Motion-planning results. The path followed by the service unit can be seen in the top figure. The lineal  $v_k$  and angular  $w_k$  velocities are shown in the middle, whereas the bottom figures show the heading (right) and the velocities  $\dot{x}_k$  and  $\dot{y}_k$  in the global coordinates of the robotic platform

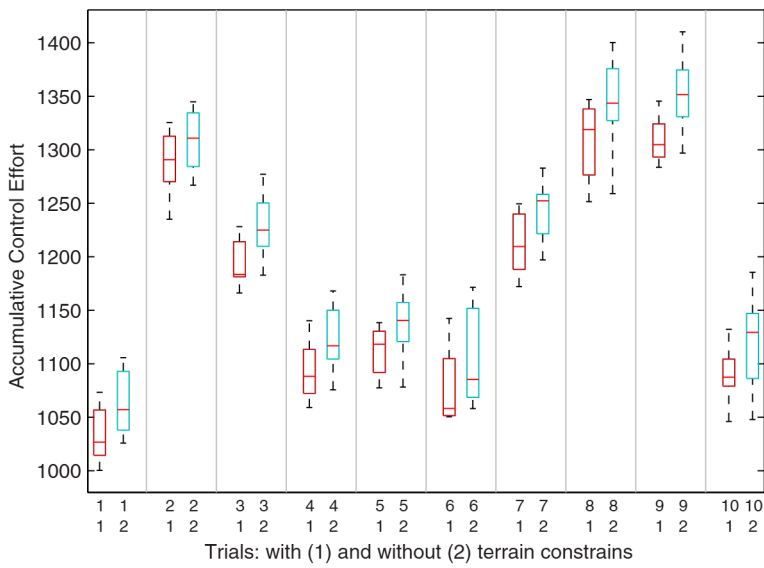


**FIGURE 8** Accumulative control effort for ten path-planning trials with and without terrain restrictions

loss with respect to the target velocity  $C_{\text{effort}} = \sum_{k=0}^{k=n} (v_k^2 + w_k^2)$ , where  $v_k$  is the linear velocity and  $w_k$  is the angular velocity at the  $k$ th waypoint, and  $n$  is the number of waypoints in the planned path. Using such a metric for the ten different trials, we obtain the results shown in Figure 8.

Figure 8 shows that the accumulative control efforts between the path traveled considering the terrain restrictions and that without considering it differ slightly from each other. However, it is worth mentioning that the difference between them is only about 5%. This means that the control actions that drove the machinery from the starting position to some harvesting point required 5% less control effort than using RRT\* without terrain considerations. Nevertheless, the accumulative path-tracking errors did not show any remarkable difference when using terrain constraints.

## 6.5 | Harvesting times

An important result to mention is the time that the vehicle was used for harvesting. For the harvesting trials shown in Section 6.1, the vehicle required only 7 h of total direct use, in contrast with the 13 h reported by the farmer when the harvesting machinery is driven by a human in a similar scenario. The latter is not trivial since our harvesting strategy might lead to a decrement in costs, mainly when machinery is rented. However, more experimentation is needed to validate such a statement.

## 7 | LESSONS LEARNED

During the field trials, several lessons were learned that will lead to further improvements in our work:

1. Since the focus of the work is a motion planner to aid harvesting tasks by reducing resources, the harvesting scheduling system proposed in Section 2.1 suffers from many drawbacks. For example,

it does not consider human factors or human-machine interaction related issues. In particular, it does not take into account that a field worker could leave the field or the task, nor does it consider the case when the yield prediction was not accurate enough. Several improvements have to be made in this system in order to make it fully functional in the harvesting process.

2. The RRT\*-based path planner using terrain constraints has been shown to save up to 5% of the accumulative controller effort if we compare it to the case without terrain restrictions. Although small, the machinery percentage might vary over the long term. It is worth mentioning, however, that the obtained results are closely related to the machinery used in this work, since the terramechanic modeling of the wheel-terrain interaction actually depends on the wheel and the vehicle.
3. The accumulative path-tracking error did not show a representative difference when using RRT\* with and without terrain restrictions. This is due to the fact that the path-tracking controller used and previously published by the authors in Ref. 24 is exponentially stable and was tested for different terrain conditions.
4. Although our harvesting scheduling system required 7 h of vehicle operation (6 h less according to what was informed by the farmer when driving the machinery for collecting beans), the scheduling algorithm, as previously stated, still needs improvement. However, such a difference in time of use might lead to two important results: the first is the lowering of costs if the machinery is rented; second, the harvested fruit achieves shelter—or deposit—in a shorter time. The latter might lead to an increment in the quality of the fruit since its sunlight exposing time decreased. Nevertheless, at this stage, more experimentation is needed.
5. Since the work presented here was focused in Hass avocado groves (which is fruit in Chile), the harvesting season corresponds to October–December, leaving a very short time to test our system in long-term experimentations.

## 8 | CONCLUSIONS

This work has presented an integrated harvesting and motion-planning strategy that uses information from previous yieldmaps, harvesting rates, and terrain traversability. The harvesting strategy yields a sequence of locations that are obtained from a solution of the travelling salesman problem, which allows us to sort the harvesting points in order of relevance according to plant yield and harvest progress, thus to minimize the time fruits are left in the field before the robot picks the bins.

The path planner considers the terrain traversability that models the efficiency losses in mobility produced by the roughness of the terrain, wheel ground interaction, the terrain deformability, and the terrain slope. The path-planning approach uses the well-known RRT\* path-planning algorithm and a novel cost function to generate the best path for the robot along the sequence of prioritized waypoints. This cost metric uses not only the total length of the path, but also the total time spent by the robot traveling as determined by the traversability measure. Results from a real grove have shown that the proposed strategy generates paths that avoid the regions that are more difficult to traverse, and hence it reduces the overall effort and time the robot takes to complete the harvest task when compared to human-driven machinery.

Our ongoing research and future work concerns the online terramechanic characterization of the terrain using active vision systems, as well as a study of the financial impact of our approach in terms of energy savings and harvesting times.

## ACKNOWLEDGMENTS

This project has been supported by the National Commission for Science and Technology Research of Chile (CONICYT) under Fondecyt grant 1140575, Fondeckip grant 120141, and grant CONICYT-PCHA/MagisterNacional/2014-22141669, and the Advanced Center of Electrical and Electronic Engineering, CONICYT, grant number FB0008.

## REFERENCES

1. Auat Cheein F, Carelli R. Agricultural robotics: Unmanned robotic service units in agricultural tasks. *Ind Electr Mag, IEEE*. 2013;7(3):48–58.
2. Zion B, Bechar A, Regev R, et al. Mechanical harvesting of olives—An operations study. *Israel J Plant Sci*. 2011;59:71–84.
3. Riveiro J, Marey M, Marco J, Alvarez C. Procedure for the classification and characterization of farms for agricultural production planning: Application in the northwest of spain. *Comput Electron Agr*. 2008;61:169–178.
4. Zhang Q, Pierce FJ. *Agricultural Automation: Fundamentals and Practices*. CRC Press; 2013.
5. Bochtis D, Griepentrog H, Vougioukas S, Busato P, Berruto R, Zhou K. Route planning for orchard operations. *Comput Electron Agr*. 2015;113:51–60.
6. Bac CW, van Henten EJ, Hemming J, Edan Y. Harvesting robots for high-value crops: State-of-the-art review and challenges ahead. *J Field Robot*. 2014;31(6):888–911.
7. Spekken M, Bruin S, Molin J, Sparovek G. Planning machine paths and row crop patterns on steep surfaces to minimize soil erosion. *Comput Elecron Agr*. 2016;124:194–210.
8. Alves Barbosa de Oliveira Vaz D, Inoue R, Grassi V. Kinodynamic motion planning of a skid-steering mobile robot using RRTs. In: *Robotics Symposium and Intelligent Robotic Meeting (LARS), 2010 Latin American*. 2010:73–78.
9. Bochtis D, Sorensen C, Vougioukas S. Path planning for in-field navigation-aiding of service units. *Comput Electron Agr*. 2010;74:80–90.
10. LaValle SM. *Planning Algorithms*. Cambridge, UK: Cambridge University Press; 2006. Available at <http://planning.cs.uiuc.edu/>.
11. LaValle S, Kuffner JJJ. Randomized kinodynamic planning. In: *1999 IEEE International Conference on Robotics and Automation, Volume 1*. 1999:473–479.
12. Karaman S, Frazzoli E. Incremental sampling-based algorithms for optimal motion planning. In: *Proceedings of Robotics: Science and Systems*. Zaragoza, Spain: 2010a.
13. Karaman S, Frazzoli E. Optimal kinodynamic motion planning using incremental sampling-based methods. In: *2010 49th IEEE Conference on Decision and Control (CDC)*. 2010b:7681–7687.
14. Bac CW, Roorda T, Reshef R, Berman S, Hemming J, van Henten EJ. Analysis of a motion planning problem for sweet-pepper harvesting in a dense obstacle environment. *Biosyst Eng*. 2016;146:85–97.
15. Wong J. *Theory of Ground Vehicles*. John Wiley & Sons; 2008.
16. Bekker M. *Introduction to Terrain-Vehicle Systems*. The University of Michigan Press; 1969.
17. Wong J-Y, Reece A. Prediction of rigid wheel performance based on the analysis of soil-wheel stresses. Part I. Performance of driven rigid wheels. *J Terramechan*. 1967;4(1):81–98.
18. Kewlani G, Ishigami G, Iagnemma K. Stochastic mobility-based path planning in uncertain environments. In: *IROS*. IEEE; 2009:1183–1189.
19. Han X, Kim H, Kim J, et al. Path-tracking simulation and field tests for an auto-guidance tillage tractor for a paddy field. *Comput Electron Agr*. 2015;112:161–171.
20. Hameed I, Bochtis D, Sorensen C, Jensen A, Larsen R. Optimized driving direction based on a three-dimensional field representation. *Comput Electron Agr*. 2013;91:145–153.
21. Auat-Cheein F. Slam-based maneuverability strategy for unmanned car-like vehicles. *Robotica, Cambridge*. 2013;31(6):905–921.
22. Ball D, Upcroft B, Wyeth G, et al. Vision-based obstacle detection and navigation for an agricultural robot. *J Field Robot*. 2016;33(8):1107–1130.
23. Auat-Cheein F, Scaglia G, Torres-Torriti M, et al. Algebraic path tracking to aid the manual harvesting of olives using an automated service unit. *BioSyst Eng*. 2016;142(2):117–132.
24. Auat Cheein F, Scaglia G. Trajectory tracking controller design for unmanned vehicles: A new methodology. *J Field Robot*. 2014;31(6):861–887.
25. Applegate DL, Bixby RE, Chvátal V, Cook WJ. *The Traveling Salesman Problem: A Computational Study*. Princeton Series in Applied Mathematics, 2nd ed. Princeton University Press; 2007.
26. Nuske S, Wilshusen K, Achar S, Yoder L, Narasimhan S, Singh S. Automated visual yield estimation in vineyards. *J Field Robot*. 2014;31(5):837–860.
27. Auat-Cheein F, Scaglia G. Laser-based trespassing prediction in restrictive environments: A linear approach. *Sensors*. 2012;12:11870–11887.
28. Garcia-Bunster G, Torres-Torriti M. A density-based approach for effective pedestrian counting at bus stops. In: *IEEE International Conference on Systems, Man and Cybernetics*. 2009:3434–3439.

29. Bienstock D, Goemans M, Simchi-Levi D, Williamson D. A note on the prize collecting traveling salesman problem. *Math Program*. 1993;59:413–420.
30. Rudd R. Estimating the mu slip curve via extended kalman filtering. *Mathematica J*. 2008;11:1.
31. Ming Q. *Sliding mode concontrol design for abs system*. Master's thesis, Virginia Polytechnic Institute and State University; 1997.
32. Li L, Wang F-Y, Zhou Q. Integrated longitudinal and lateral tire/road friction modeling and monitoring for vehicle motion control. *IEEE Transactions on Intelligent Transportation Systems*. 2006;7(1):1–19.
33. Marin L, Valles M, Soriano A, Valera A, Albertos P. Multi sensor fusion framework for indoor-outdoor localization of limited resource mobile robots. *Sensors (Basel)*. 2013;13:14133–14160.
34. Adiyatov O, Varol H. Rapidly-exploring random tree based memory efficient motion planning. In: 2013 IEEE International Conference on Mechatronics and Automation. 2013:354–359.

**How to cite this article:** Auat Cheein F, Torres-Torriti M, Hopfenblatt NB, Prado AJ, Calabi D. Agricultural service unit motion planning under harvesting scheduling and terrain constraints. *J Field Robotics*. 2017;34:1531–1542.  
<https://doi.org/10.1002/rob.21738>